Inorganic Chemistry

Article

pubs.acs.org/IC

# Iron in a Trigonal Tris(alkoxide) Ligand Environment

Matthew B. Chambers,[†] Stanislav Groysman,[†,§] Dino Villagrán,[†,∥] and Daniel G. Nocera*[,†,‡]

[†]Department of Chemistry, 6-335, Massachusetts Institute of Technology, 77 Massachusetts Avenue, Cambridge, Massachusetts 02139-4307, United States

[‡]Department of Chemistry and Chemical Biology, Harvard University, 12 Oxford Street, Cambridge, Massachusetts 02138-2902, United States

Supporting Information

**ABSTRACT:** Mononuclear Fe(II) and Fe(III) complexes residing in a trigonal tris(ditox) (ditox = $^{t}Bu_2(Me)CO^-$) ligand environment have been synthesized and characterized. The Fe(III) ditox complex does not react with oxidants such as PhIO, whereas $NMe_3O$ substitutes a coordinated tetrahydrofuran (THF) in the apical position without undergoing oxo transfer. In contrast, the Fe(II) ditox complex reacts rapidly with PhIO or $Me_3NO$ in THF or cyclohexadiene to furnish a highly reactive intermediate, which cleaves C−H bonds to afford the Fe(III)−hydroxide complex. When generated in 1,2-difluorobenze, this intermediate can be intercepted to oxidize phosphines to phosphine oxide. The fast rates at which these reactions occur is attributed to a particularly weak ligand field imparted by the tris(alkoxide) ancillary ligand environment.


## INTRODUCTION

High valent iron-oxo moieties are important intermediates in critical oxidation processes in nature including the activation of C−H bonds.[1−4] This hallmark reactivity of iron based enzymes provides an imperative for the syntheses of iron-oxo complexes with the aim of engendering an efficient and potent oxidation chemistry.[5] Though originally elusive,[6] mononuclear species containing nonheme Fe(IV)-oxo functionalities have now been realized[7] with high valent iron centers supported in tetragonal[8−14] and trigonal bipyramidal[15−21] ligand fields. The majority of these complexes feature a primary coordination sphere comprising four or five coordinate polydentate nitrogen donors. The ligand field of the Fe(IV)-oxo functionality is particularly important in tuning the spin state of the metal center. A key feature to the reactivity of nonheme Fe(IV)-oxo complexes is the accessibility of a quintet high spin state. Whereas Fe(IV)-oxo complexes can be isolated in the intermediate triplet spin state,[9] supporting density functional theory (DFT) calculations suggest that a thermally accessible quintet state affords the minimum barrier toward C−H bond activation.[22,23] As such, ligand modifications have afforded more accessible high spin states, and in some cases a high spin ground state, with faster rates of reaction observed.[24−26] In view of our interest in the use of metal-oxo complexes to promote energy conversion reactions,[27,28] we have explored the coordination chemistry of metals in the exceptionally weak ligand field engendered by the tris(alkoxide) platform of ditox (ditoxH = $^{t}Bu_2MeCOH$).[29] The steric bulk of ditox is reduced relative to its tritox[30,31] brethren by virtue of the replacement of one $^{t}Bu$ group by Me. Ditox enables the preferential formation of tris(alkoxide) metal complexes, as we have recently demonstrated for 3d transition metals (M = V, Cr). Such an alkoxide ligand platform provides an oxidation-resistant ligand environment of very weak field. Spectroscopic, structural, computational, and reactivity studies on the pseudo-tetrahedral $d^0$−$d^2$ $[M(ditox)_3O]$ (M = V, Cr) oxo complexes have demonstrated that the d electrons occupy metal-oxo $\pi^*$ orbitals with all frontier orbitals possessing significant oxo character. Thus, a tris(ditox) metal-oxo system possessing more than two d electrons is expected to be highly reactive as a result of substantial unpaired electron density on the oxo.

We examine this proposition here by elaborating the iron chemistry of the tris(ditox) platform. Whereas Fe(III) in the ditox ligand field is recalcitrant to oxidation, we demonstrate that Fe(II) undergoes facile reaction with oxygen−transfer reagents to form highly reactive intermediates, which readily activate C−H bonds to afford tetrahedral Fe(III)-hydroxide complexes.

## EXPERIMENTAL SECTION

**General Considerations.** All reactions involving air-sensitive materials were performed in a nitrogen-filled glovebox. Solvents were purified using SG Water Glass Contour Solvent System and stored over 4 Å molecular sieves. Compounds were routinely characterized by IR, elemental analyses, and the X-ray analysis; selected compounds were characterized by NMR, cyclic voltammetry (CV), and electrospray ionization mass spectrometry (ESI-MS). IR spectra of powdered samples were recorded on a PerkinElmer Spectrum 400 FT-IR/FT-FIR Spectrometer outfitted with a Pike Technologies GladiATR attenuated total reflectance accessory with a monolithic diamond crystal stage and pressure clamp. CV experiments were performed using a glassy carbon working electrode (0.07 $cm^2$), a platinum wire auxiliary electrode, and a $Ag/AgNO_3$ (0.1 M) reference electrode in 0.1 M $NBu_4PF_6$ acetonitrile/tetrahydrofuran (THF)

Received: December 1, 2012

   dx.doi.org/10.1021/ic302634q | Inorg. Chem. XXXX, XXX, XXX−XXX

solutions at room temperature using a BASI CV50W in a glovebox. The potentials were referenced to the ferrocene/ferrocenium couple by recording the CV of ferrocene before and after each scan. All NMR spectra were recorded at the MIT Department of Chemistry Instrumentation Facility on a Varian Mercury 300 NMR spectrometer in $C_6D_6$ at room temperature. Magnetic moments were determined in $C_6D_6$ at room temperature on a Varian Mercury 300 NMR Spectrometer using the Evans method.[32] Pascal constants were used to estimate diamagnetic correction. Silylated glassware was obtained by swirling the reaction vessels with $Me_3SiCl$ and drying them thereafter under vacuum. UV−vis measurements were recorded on a Varian Cary 5000 spectrometer and references to appropriate solvent. All UV−vis measurements were performed on sample in solutions of THF. Elemental analyses were performed by Midwest Microlab LLC. Methyl lithium (1.6 M in ether), 2,2,4,4-tetramethyl-3-pentanone, 15-crown-5-ether, $FeCl_3$, and $FeCl_2$ were purchased from Aldrich. PhIO was purchased from Alfa Aesar. $ONMe_3$ was purchased from Aldrich and sublimed twice before use. $^tBu_2MeCOLi$ and $^tBu_2MeCOH$ (Liditox and Hditox hereafter) were prepared according to literature procedures.[33]

**Preparation of Compounds. $^tBu_2MeCOK$ (Kditox).** A 3.000 g portion (18.95 mmol) of Hditox was added as a solid in small portions over the course of 15 min to a solution of ether (50 mL) that contained 0.836 g (20.9 mmol) of KH. The solution was stirred for 15 min. The resulting white slurry was allowed to stir at room temperature for 6 h or longer until gas evolution subsided. Diethyl ether solution was filtered through Celite and volatiles were removed in vacuo. Resulting white solid was extracted with pentane/diethyl ether mixture (5:1, ca. 20 mL) and was filtered through Celite. The colorless solution was concentrated to about 4 mL and left to stand at −40 °C for 12 h. Colorless crystals were obtained, collected, and dried in vacuo (94.99% yield, 3.530 g, 18.00 mmol). Anal. Calcd. (Found) for $C_{10}H_{21}KO$: C, 60.25 (59.82); H, 12.11 (11.33). $^1H$ NMR ($C_6D_6$, 300 MHz) $\delta$ 1.10 (s, $^t$Bu), 0.96 (s, Me). IR ($cm^{-1}$): 1478 (m), 1389 (m), 1381 (m), 1360 (m), 1115 (s), 1084 (s), 1013 (sh), 996 (m), 945 (m), 926 (m), 897 (m), 877 (sh), 831 (sh), 675 (m), 649 (m), 583 (s), 560 (m), 537 (w), 495 (s).

**Fe(ditox)$_3$(THF) (1).** A 271 mg portion (1.65 mmol) of Liditox was dissolved in ether (2 mL) and was added to the orange solution of 89 mg (0.55 mmol) of $FeCl_3$ in THF (2 mL). White solid formed immediately. The solution was stirred for 30 min, filtered, and the solvents were removed. The residue was extracted with pentane (1 mL), filtered, and the solution was stored at −40 °C. The product was obtained as yellow crystals in two crops (64% yield, 210 mg, 0.35 mmol). Anal. Calcd (Found) for $C_{34}H_{71}O_4Fe$: C, 68.09 (68.01); H, 11.93 (11.52). $^1H$ NMR ($C_6D_6$, 300 MHz) $\delta$ 19.2. (br s, $^t$Bu), IR ($cm^{-1}$): 1474 (m), 1390 (sh), 1385 (m), 1364 (m), 1095 (sh), 1081 (vs), 1017 (sh), 1001 (s), 936 (s), 916 (vs), 868 (s), 686 (s), 590 (m), 546 (w), 532 (w). No discernible features in UV−vis spectrum. $\mu_{eff}$ = 5.09 $\mu$B. Alternatively, **1** could be prepared from Fe(ditox)$_3$Li($OEt_2$). $AgPF_6$ (41 mg) was dissolved in 2 mL of THF and added to the stirred pale blue-green solution of Fe(OR)$_3$Li($OEt_2$) (98.0 mg, 0.161 mmol) in ether (1 mL). The solution turned dark brown, and it was stirred for 1 h, filtered, and the solvent was removed in vacuo. The brown residue was extracted with pentane (1 mL, yellow-brown solution), and left to stand at −40 °C. The product was obtained as yellow crystals in two crops (60% yield, 58 mg, 0.097 mmol).

**Fe(ditox)$_3$Li($OEt_2$) (2).** A 271 mg portion (1.65 mmol) of Liditox in 2 mL of ether was added in one portion to the stirred off-white ether suspension (2 mL) of $FeCl_2$ (89.0 mg, 1.55 mmol), and the reaction was left to stir overnight. The resulting brown solution was filtered and concentrated. A light blue-green solid was recrystallized from pentane (2 mL) at −40 °C, to give [Fe(ditox)$_3$Li($OEt_2$)] in 62.5% yield (210 mg, 0.344 mmol). Anal. Calcd. (Found) for $C_{34}H_{73}FeLiO_4$: C, 67.08 (66.80); H, 12.09 (11.90). IR ($cm^{-1}$): 1391 (w), 1383 (m), 1370 (m), 1359 (m), 1178 (w), 1127 (m), 1103 (m), 1089 (s), 1062 (s), 1014 (m), 999 (s), 943 (m), 931 (m), 907 (s), 866 (w), 832 (w), 793 (w), 684 (m), 646 (m), 585 (s), 564 (m), 515 (br, m), 489 (m UV−vis, $\lambda_{max}$ ($\varepsilon$): 748 nm (71 $M^{-1}$ $cm^{-1}$). $\mu_{eff}$ = 4.68 $\mu$B.

**Fe(ditox)$_3$Li(THF) (3).** A 725 mg portion (4.42 mmol) of Liditox in 3 mL of THF was added in one portion to the stirred off-white THF slurry (2 mL) of $FeCl_2$ (186 mg, 1.47 mmol). The solution became homogeneous and assumed a green color. After 1 h, volatiles were removed, and the residue was extracted with pentane (3 mL). Pentane solution was concentrated to about 1 mL, and left at −40 °C for 12 h to give [Fe(ditox)$_3$Li(THF)] in 70.7% yield (627 mg, 1.04 mmol). Anal. Calcd. (Found) for $C_{34}H_{73}FeLiO_4$: C, 67.31 (67.21); H, 11.80 (11.61). IR ($cm^{-1}$): 1482 (m), 1472 (m), 1391 (w), 1382 (m), 1372 (m), 1361 (m), 1131 (m), 1111 (s), 1094 (s), 1036 (m), 1021 (m), 1009 (m), 1000 (m), 940 (m), 932 (m), 910 (s), 885 (m), 870 (m), 681 (m), 649 (m), 586 (s), 567 (sh), 520 (br, m), 468 (w), 453 (w). UV−vis, $\lambda_{max}$ ($\varepsilon$): 748 nm (71 $M^{-1}$ $cm^{-1}$). $\mu_{eff}$ = 4.66 $\mu$B

**Fe(ditox)$_3$K(THF)$_2$ (4).** A 1.00 g portion (5.09 mmol) of Kditox in 3 mL of THF was added in one portion to the stirred pale yellow THF slurry (2 mL) of $FeBr_2$ (366 mg, 1.70 mmol). The solution became homogeneous and assumed a green color. After 2 h, volatiles were removed, and the residue was extracted with pentane (5 mL) and filtered through Celite. The pentane solution was collected and concentrated to about 1 mL, and left to stand at −40 °C for 24 h to give **4** in 67.2% yield (810 mg, 1.14 mmol). Anal. Calcd. (Found) for $C_{38}H_{79}FeKO_5$: C, 64.19 (63.89); H, 11.20 (10.96). IR ($cm^{-1}$): 1483 (m), 1393 (sh), 1383 (m), 1358 (m), 1214 (w), 1128 (s), 1106 (s), 1074 (vs), 1051 (vs), 1009 (vs), 976 (s), 894 (w), 839 (m), 819 (m), 796 (s), 635 (m), 621 (m), 569 (s), 537 (w), 526 (w). UV−vis: 748 nm (71 $M^{-1}$ $cm^{-1}$). UV−vis, $\lambda_{max}$ ($\varepsilon$): 773 nm (90 $M^{-1}$ $cm^{-1}$). $\mu_{eff}$ = 4.71 $\mu$B.

**[Fe(ditox)$_3$][K(15-crown-5-ether)$_2$] (5).** A 750 mg portion (1.05 mmol) of Fe(ditox)$_3$K($THF)_2$ was dissolved in 7 mL of pentane. To the solution an excess of 15-crown-5-ether was added (ca. 2 mL, 10.1 mmol) at room temperature and immediately a light green precipitate formed. The reaction mixture was stirred as a light green slurry for 30 min. Stirring ceased and a light green solid was allowed to settle to the bottom of the reaction vessel. A colorless supernatant was removed via pipet. The remaining solid was washed 3 × 5 mL of pentane. The light green solid was dissolved in diethyl ether (8 mL) and filtered through Celite. Diethyl ether solution was collected and concentrated to about 1 mL and left at −40 °C for 24 h to give **5** in 85% yield (907 mg, 0.89 mmol). Anal. Calcd. (Found) for $C_{50}H_{103}FeKO_{13}$: C, 59.62 (59.96); H, 10.02 (10.31). IR ($cm^{-1}$): 1475 (m), 1401 (m), 1378 (sh), 1352 (m), 1303 (m), 1289 (s), 1250 (br, m), 1201 (w), 1118 (vs), 1090 (vs), 1052 (sh), 1040 (s), 1016 (s), 976 (s), 940 (s), 855 (s), 830 (m), 806 (s), 691 (w), 667 (w), 632 (m), 576 (m), 547 (m), 519 (m), 508 (m). UV−vis, $\lambda_{max}$ ($\varepsilon$): 798 nm (98 $M^{-1}$ $cm^{-1}$). $\mu_{eff}$ = 4.75 $\mu$B.

**Fe(ditox)$_3$($ONMe_3$) (6).** A 7.0 mg portion (0.088 mmol) of $Me_3NO$ was dissolved in 2 mL of THF and added to the stirred yellow solution of **1** (26.0 mg, 0.044 mmol) in 2 mL of ether. The resulting yellow solution was stirred for 1 h, filtered, and the volatiles were removed in vacuo. A yellow-brown residue was extracted with 2 mL of ether, filtered, and the solution was concentrated to about 0.5 mL volume. Yellow crystals of **6** are obtained from solution at −40 °C for 24 h in 80% yield (21 mg, 0.035 mmol). Anal. Calcd. (Found) for $C_{33}H_{72}NO_4Fe$: C, 65.75 (65.65); H, 12.04 (11.81); N, 2.32 (2.10). IR ($cm^{-1}$): 1395 (w), 1386 (m), 1367 (m), 1236 (w), 1099 (vs), 1088 (vs), 1004 (s, C−O), 939 (s), 923 (s), 870 (w), 767 (m), 704 (m), 686 (m), 598 (m), 549 (m), 477 (m). No discernible features in the UV−vis spectrum. $\mu_{eff}$ = 6.10 $\mu$B.

**Fe(ditox)$_3$(OH)Li($THF)_n$, $n$ = 3 (7), $n$ = 2 (7a), $n$ = 0 (7b) and Fe(ditox)$_3$(OH)Li(di-THF) (8).** Solid iodosyl benzene (74.0 mg, 0.337 mmol) was added to the stirred green solution of 204 mg (0.337 mmol) of **3** in 3 mL of THF. The resulting heterogeneous mixture quickly became homogeneous (ca. 30 s), and the initial brown solution turned yellow-orange (ca. 1 min). After 2 min, volatiles were removed in vacuo. The resulting mixture was extracted with pentane (3 mL). Crystallization from pentane leads to the formation of 61 mg (0.088 mmol, 23%) of yellow crystals of **8** in two crops. Anal. Calcd. (Found) for $C_{42}H_{88}FeLiO_7$: C, 65.78 (65.41); H, 11.33(11.23). IR ($cm^{-1}$): 3630 (OH), 1386 (w), 1362 (w), 1084 (vs), 1000 (s), 931 (m), 911 (s), 866 (w), 793 (m), 683 (m), 654 (w), 595 (m), 568 (w), 529 (br, m), 471 (m), 451 (w). ESI−$MS^+$ ($m/z$) 143.1 [di-THF + H]$^+$, 291.1


dx.doi.org/10.1021/ic302634q | Inorg. Chem. XXXX, XXX, XXX−XXX

$[(di\text{-}THF)_2Li]^+$ ESI−MS$^-$ ($m/z$) 405.3 $[Fe(ditox)_2(OH)(OH_2)]^-$, 562.4 $[(Fe(ditox)_3(OH)(OH_2)]^-$. UV−vis: no notable features.

The crude insoluble solid was taken up from pentane in a mixture of ether/THF (3:1 mL). Slow evaporation of the solution yields 76 mg of a mixture of **7** and **7a** as yellow crystals (0.096 mmol, ca. 25% yield). The identity of the major product (ca. 90%), containing three THF molecules ($Fe(ditox)_3(OH)Li(THF)_3$) (**7**), and the minor product (ca. 10%) containing two THF molecules ($Fe(ditox)_3(OH)Li(THF)_2$) (**7a**) was proven by X-ray diffraction (XRD), and confirmed by IR. The non-dried sample of the mixture of **7** and **7a**, covered with Paratone N−oil, contains mostly pure **7** (by unit cell determination). The presence of **7a** in a dried sample of **7** is signified by two OH resonances in the IR spectrum at 3630 cm$^{-1}$ and 3700 cm$^{-1}$. Exposure of the bright yellow transparent crystals of **7** to vacuum leads to an immediate loss of crystallinity. The IR of the dried material shows two peaks at 3700 cm$^{-1}$ and 3630 cm$^{-1}$. Prolonged drying under vacuum or crystallization of the compound from THF-deficient solution (ca. 3:0.2 mL ether:THF) increases the amount of $Fe(ditox)_3(OH)Li(THF)_2$ (**7a**) as determined by IR. **7** and **7a** cannot be separated completely as the recrystallization of **7**/**7a** in the absence of THF forms $[Fe(ditox)_3(OH)Li]_2$ (**7b**) in low yield.

Solid iodosobenzene (46.0 mg, 0.205 mmol) was added to the stirred green solution of 126 mg (0.205 mmol) of $Fe(ditox)_3Li(THF\text{-}d_8)$, **3-d$^8$THF**, and 330.0 mg (4.125 mmol, ca. 20.12 equiv) of 1,4-cyclohexadiene in 3 mL of THF. The resulting heterogeneous mixture quickly became homogeneous (ca. 30 s), and bright yellow (ca. 1 min). After 1 min, volatiles were removed in vacuo. The resulting mixture was extracted with pentane/THF (3 × 0.5 mL) mixture. Concentration of the solvent under vacuum to about 0.5 mL led to the formation of yellow crystals. Crystals were dried to give $Fe(ditox)_3(OH)Li(THF)_3$ **7** and about 10% $Fe(ditox)_3(\mu_2\text{-}OH)Li(THF)_2$ **7a** in about 92% yield (145 mg, 0.189 mmol).

*Characterization of 7/7a.* ESI−MS$^-$ ($m/z$) 544.2 $[Fe(ditox)_3(OH)]^-$, 562.4 $[(Fe(ditox)_3(OH)(OH_2)]^-$ Anal. Calcd. (Found) for $C_{42}H_{88}FeLiO_7$: C, 65.69 (64.40); H, 11.55 (11.21). Repeated attempts to obtain EA showed low percent of C, consistent with the loss of THF and/or decomposition. IR (cm$^{-1}$): 3700(w), 3630 (w), 1391 (w), 1383 (m), 1370 (m), 1359 (m), 1178 (w), 1127 (m), 1103 (m), 1089 (s), 1062 (s), 1014 (m), 999 (s), 943 (m), 931 (m), 907 (s), 866 (w), 832 (w), 793 (w), 684 (m), 646 (m), 585 (s), 564 (m), 515 (br, m), 489 (m). No discernible features in the UV−vis spectrum.

**$[Fe(ditox)_3(OH)][K(15\text{-}crown\text{-}5\text{-}ether)_2]$ (9).** Solid iodosyl benzene (108 mg, 0.492 mmol) was added to the stirred green solution of 500 mg (0.492 mmol) of **5** in 6 mL of THF. The resulting heterogeneous mixture quickly became homogeneous (ca. 1 min), and turned yellow-orange. After 2 min, volatiles were removed in vacuo. The resulting mixture was washed 3 × 5 mL of pentane each time. The remaining solid was extracted with a diethyl ether/THF mixture (5 × 1 mL) and filtered through Celite. The yellow-orange solution was concentrated to about 1 mL and left to stand at −40 °C for 24 h to yield pale yellow crystals. Crystals were collected and dried in vacuo to give **9** in 65.8% yield (335 mg, 0.324 mmol). An alternative method of preparation involves the use of $Me_3NO$ in place of PhIO in the same molar ratios reported. Anal. Calcd. (Found) for $C_{50}H_{104}FeKO_{14}$: C, 58.63 (58.66); H, 10.23 (9.91). IR (cm$^{-1}$): 1484 (m), 1476 (sh), 1443 (w), 1383 (m), 1372 (sh), 1355 (s), 1303 (m), 1290 (m), 1253 (m), 1245 (m), 1120 (vs), 1105 (sh), 1092 (sh), 1079 (vs), 1053 (sh), 1042 (s), 1014 (s), 979 (s), 941 (s), 907 (sh), 856 (s), 830 (m), 808 (s), 667 (sh), 635 (s), 577 (s), 543 (br, s), 530 (sh), 411 (sh), 462 (vw). No discernible features in UV−vis spectrum. $\mu_{eff}$ = 6.10 $\mu$B.

**X-ray Crystallographic Details.** Crystals were mounted on a Bruker three circle goniometer platform equipped with an APEX detector. A graphite monochromator was employed for wavelength selection of the Mo K$\alpha$ radiation ($\lambda$ = 0.71073 Å). Data were processed and refined using the program SAINT supplied by Siemens Industrial Automation. Structures were solved by direct methods in SHELXS and refined by standard difference Fourier techniques in the SHELXTL program suite (6.10 v., Sheldrick G. M., and Siemens Industrial Automation, 2000). Hydrogen atoms were placed in calculated positions using the standard riding model and refined isotropically; all other atoms were refined anisotropically. The structure of **4** had one disordered THF molecule that was satisfactorily modeled. The structure of **7** contains four molecules of disordered solvent for one molecule of the metal complex, which leads to the overall low quality of the structure. Three molecules were modeled, whereas the fourth could not be modeled satisfactorily. Therefore, electron density associated with the disordered solvent was removed using the SQUEEZE program. PLATON indicated pseudo-trigonal symmetry ($P\bar{3}$) for **7**. In the structure of **9**, both the 15-crown-5-ether molecules were disordered. One of the 15-crown-5-ether was successfully modeled. However, heavy restraints on the anisotropy of several carbon atoms of the 15-crown-5-ether molecule interacting with the Fe−OH had to be utilized for the minor orientation. The Fe−OH hydrogen atom was detected from the electron density difference map for structure **9**. In the structure of **8** two enantiomers of di-THF ligand co-crystallize at the same position. In the structures of **3**, **7**, **8**, and **9**, some of the $^t$Bu groups were disordered; the disorder was modeled satisfactorily in separate parts.

**Computational Details.** Density functional theory (DFT) calculations were performed with the hybrid functional Becke-3 parameter exchange functional[34] and the Lee−Yang−Parr nonlocal correlation functional (B3LYP)[35] as implemented in the Gaussian 03, Revision B.05 software package.[36] An effective core potential (ECP) representing the 1s2s2p core was used for iron (LANL2DZ).[37] The double-$\zeta$ quality correlation-consistent polarized ccc-pvdz basis set by Dunning and co-workers was used on all oxygen atoms, while double-$\zeta$ quality basis sets (D95) were used on carbon and hydrogen.[38]

The calculations were performed on simplified models of $[Fe(ditox)_3(O)]^-$ and $LiFe(ditox)_3(O)$ where the $^t$Bu groups are replaced by methyl groups. All geometries were confirmed as local minima structures by calculating the Hessians and checking that no negative eigenvalues were present. Supporting Information, Figure S30 pictorially depicts the calculated spin density for the models of $[Fe(ditox)_3(O)]^-$ and $LiFe(ditox)_3(O)$. Supporting Information, Tables S5−S7 list the Cartesian coordinates of the optimized geometries of the models of $[Fe(ditox)_3(O)]^-$ and $LiFe(ditox)_3(O)$ and the quintet, triplet, and singlet multiplicities.

## RESULTS

**Synthesis and Characterization of Fe Ditox Compounds.** The preparative reaction chemistry employed to obtain the iron ditox compounds is illustrated in Figure 1. Homoleptic iron tris(alkoxide) complexes were prepared by salt metathesis reactions between corresponding iron halides and alkali metal alkoxides. The reaction of 3 equiv of Li(ditox) or K(ditox) with $FeCl_3$ in THF at room temperature, (eq 1,

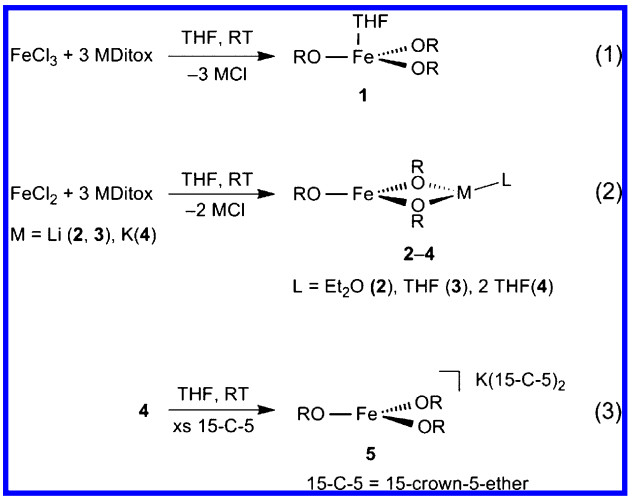


**Figure 1.** Preparative reactions of Fe ditox compounds.


dx.doi.org/10.1021/ic302634q | Inorg. Chem. XXXX, XXX, XXX−XXX

Figure 1) affords a white precipitate and a yellow solution of Fe(ditox)$_3$THF (**1**). Filtration followed by recrystallization from pentane at −30 °C yields analytically pure products in 64% yield for Li(ditox) and 71% yield for K(ditox).

Treatment of 3 equiv of Li(ditox) with $FeCl_2$ in THF or diethyl ether at room temperature results in the formation of a green solution of Fe(ditox)$_3$Li(L) (L = diethyl ether (**2**), THF (**3**)) in 63% and 71% yields, respectively, after filtration and recrystallization from pentane (eq 2, Figure 1). The potassium analogue, Fe(ditox)$_3$K(THF)$_2$ (**4**) was obtained in 67% yield using K(ditox). Of note, the alkali cation of **2**−**4** is coordinated by two ditox ligands. The trigonal planar complex [Fe(ditox)$_3$]$^-$ can be generated by treatment of **4** with excess 15-crown-5-ether resulting in [Fe(ditox)$_3$][K(15C5)$_2$] (**5**) upon recrystallization from diethyl ether in 85% yield (eq 3, Figure 1). Attempts to sequester Li cation from **2** or **3** proved more problematic. As such, **5** was exclusively used as an anionic mononuclear trigonal planar iron tris(alkoxide) synthon. Treatment of **4** with 18-crown-6-ether, a more commonly used reagent for potassium sequestration, was not effective for removal of potassium.

Single crystal XRD studies were performed on compounds **1**, **3**−**5**. Compound **1** is shown to be a distorted trigonal monopyramid with a THF molecule coordinating the axial position (Figure 2); the structure of the compound is

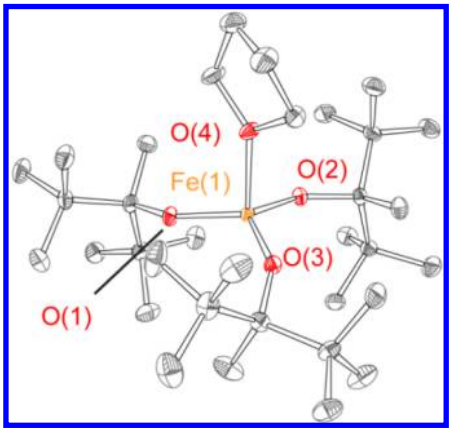


**Figure 2.** Structure of Fe(ditox)$_3$THF (**1**), 50% probability ellipsoids. H atoms are omitted for clarity. Selected bond distances: $d$(Fe1−O1) = 1.822(2) Å, $d$(Fe1−O2) = 1.823(2) Å, $d$(Fe1−O3) = 1.826(2) Å, $d$(Fe1−O4) = 2.089(2) Å. Selected bond angles: ∠(O1−Fe1−O2) = 113.4(1)°, ∠(O1−Fe1−O3) = 119.8(1)°, ∠(O2−Fe1−O3) = 118.8(1)°, ∠(O1−Fe1−O4) = 102.4(1)°, ∠(O2−Fe1−O4) = 101.1(1)°, ∠(O3−Fe1−O4) = 95.0(1)°.

isomorphous with the previously reported V(ditox)$_3$THF.[29] The average $d$(Fe−O$_{alk}$) is 1.82 Å. The alkoxide−iron bond angle is slightly distorted from an idealized trigonal planar angle of 120°, ∠(O1$_{alk}$−Fe−O2$_{alk}$) = 113°, with the apical THF molecule slightly positioned over this contracted angle. The other two ∠(O$_{alk}$−Fe−O$_{alk}$) angles are refined to 119° and 120° resulting in a sum of the angles equal to 352°, indicating that the coordinated THF results in an iron atom that is slightly above the plane of the ditox ligands.

Fe(II) complexes **3** and **4** (Figures 3 and 4, respectively) assume a Y-shaped geometry with alkali cations coordinated directly to two ditox ligands. The average $d$(Fe−O$_{alk}$) bond distance of the alkoxides coordinated to the alkali cation increase to 1.91 Å when compared to **1**. The terminally bound

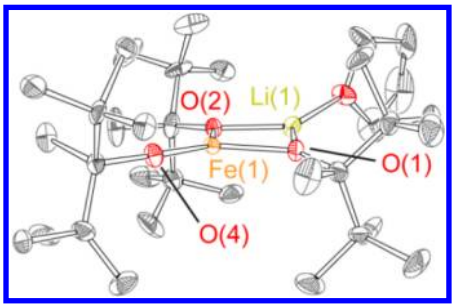


**Figure 3.** Structure of Fe(ditox)$_3$Li(THF) (**3**), 50% probability ellipsoids. Hydrogen atoms omitted for clarity. Selected bond distances: $d$(Fe1−O1) = 1.912(4) Å, $d$(Fe1−O2) = 1.922(4) Å, $d$(Fe1−O4) = 1.796(1) Å, $d$(Li1−O1) = 1.863(12) Å, $d$(Li1−O2) = 1.859(12) Å, $d$(Li1−O3) = 1.902(4) Å Selected bond angles: ∠(O1−Fe1−O2) = 88.9(1)°, ∠(O1−Fe1−O4) = 135.6(2)°, ∠(O2−Fe1−O4) = 135.6(2)°.

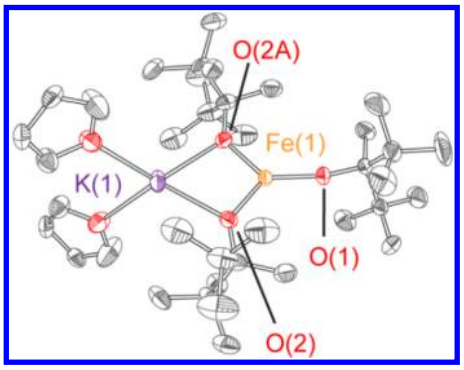


**Figure 4.** Structure of Fe(ditox)$_3$K(THF)$_2$ (**4**), 50% probability ellipsoids. H atoms are omitted for clarity. Selected bond distances: $d$(Fe1−O1) = 1.826(2) Å, $d$(Fe1−O2) = 1.903(1) Å, $d$(K1−O2) = 2.585(1) Å. Selected bond angles: ∠(O1−Fe1−O2) = 130.1(1)°, ∠(K1−O2−Fe1) = 95.8(1)°, ∠(O2−Fe1−O2A) = 99.8(1)°.

alkoxide ligands in **3** have a bond length that is 1.80 Å, shorter than that found in **1**, whereas the bond length of the terminal alkoxide of **4** is slightly elongated to 1.83 Å. Since the bond lengths of the alkoxides coordinated to the cations are essentially identical in **3** and **4**, the differences in bond lengths of the terminal alkoxide ligand of these complexes likely arise from the Y-shaped distortion owing to the size of the alkali metal cation. The contracted bond angle of **3** is 90° whereas the contracted bond angle of **4** is 100°. In both **3** and **4**, the sum of all the angles are exactly 360°, indicating that the Fe atom resides in the plane of the alkoxides for both complexes. In the absence of an alkali metal cation template, no distortion is observed. The crystal structure of **5** is shown in Figure 5. All three bond angles of **5** are 120° and $d_{avg}$(Fe−O$_{alk}$) = 1.87 Å.

The M−OR stretching region in the FTIR of **5** shows two strong absorptions at 632 cm$^{-1}$ and 576 cm$^{-1}$. As is expected upon oxidation, these features shift to higher energy in **1** to 686 cm$^{-1}$ and 590 cm$^{-1}$. Upon coordination of a potassium cation in **4**, with concomitant contraction of one of the of ∠(O$_{alk}$−Fe−O$_{alk}$) angles to 100°, the higher energy band splits into two peaks that are separated by 14 cm$^{-1}$. With Li coordination in **3** and further angle contraction, this splitting increases to 32 cm$^{-1}$. Thus the contraction of the ∠(O$_{alk}$−Fe−O$_{alk}$) angle appears to be correlated with the higher energy M−OR stretching feature.

Solution magnetic measurement (Evans method) is consistent with a high spin electronic ground state for **1**−**5**. The


dx.doi.org/10.1021/ic302634q | Inorg. Chem. XXXX, XXX, XXX−XXX

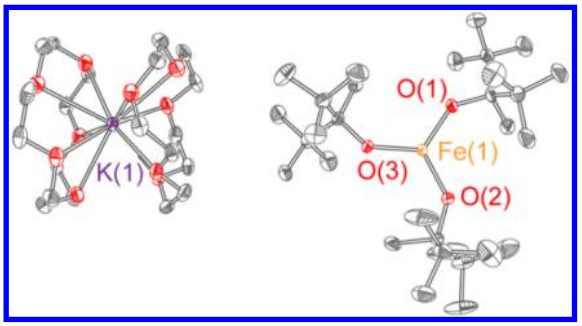


**Figure 5.** Structure of $[Fe(ditox)_3][K(15C5)_2]$, (**5**), 50% probability ellipsoids. Hydrogen atoms omitted for clarity. Selected bond distances: $d$(Fe1−O1) = 1.864(2) Å, $d$(Fe1−O2) = 1.870(2) Å, $d$(Fe1−O3) = 1.865(2) Å. Selected bond angles: ∠(O1−Fe1−O2) = 120.2(1)°, ∠(O1−Fe1−O3) = 120.1(1)°, ∠(O2−Fe1−O3) = 119.6(1)°.

room temperature magnetic moment of **1** is $\mu_{eff}$ = 5.09 $\mu_B$, which is slightly lower than the spin-only value for a $d^5$ ion but comparable to other high spin Fe(III) systems. The room temperature solution magnetic moments of $\mu_{eff}$ = 4.70 $\mu_B$ for the series of Fe(II) compounds (**2**−**5**) are consistent with high spin $S$ = 2 metal centers.

**Oxidation Chemistry.** The electrochemical behavior of **1**, **3**, and **5** is summarized in Scheme 1. Cyclic voltammograms of

**Scheme 1. Electrochemical Behavior of Fe Ditox Complexes**

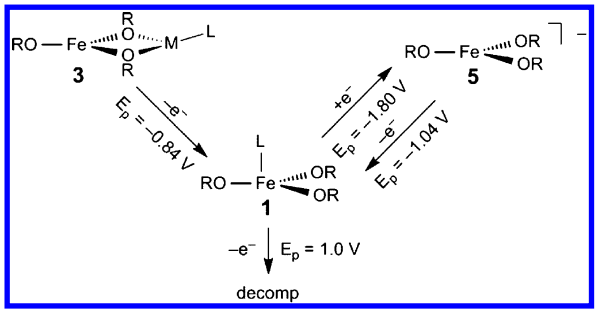


**3**, $Fe(ditox)_3Li(THF)$, in a 0.1 M $TBAPF_6$/THF solution, show a broad irreversible oxidation wave with a peak current at −0.84 V vs $FeCp_2/FeCp_2^+$ attributable to the Fe(III)/Fe(II) couple and loss of coordinated lithium. **5** displays a sharper irreversible oxidation wave with a peak current at −1.04 V vs $FeCp_2/FeCp_2^+$. The cathodic shift of the electrochemical oxidation of **5** as compared to **3** indicates that the removal of the bound lithium cation and subsequent bond angle changes requires about 200 mV of overpotential.

Upon completion of an anodic sweep wherein **3** and **5** have been electrochemically oxidized, a subsequent cathodic sweep shows a broad irreversible feature for both complexes with peak potential at −1.80 V vs $FeCp_2/FeCp_2^+$. The identical cathodic feature is observed upon the reduction of independently prepared **1**, $Fe(ditox)_3$, suggesting that the electrochemical oxidation of either **3** or **5** result in the formation **1**. The process is consistent with electrochemical irreversibility owing to the weak coordination of ligands in the apical position of **1**.

At more anodic potentials, **3** and **5** exhibit a sharp irreversible feature at 1.0 V versus $FeCp_2/FeCp_2^+$. The electrochemistry is consistent with the oxidation of the Fe(III) complex; the resulting product quickly decomposes. Notably, **1** also shows a similarly sharp irreversible oxidation at the same potential. It appears therefore that the formation of Fe(IV) in this system is feasible even in the absence of a strongly donating apical ligand.

Attempts to attain a high valent Fe-oxo species focused on the reactivity of Fe(II) and Fe(III) tris(ditox) complexes with common oxo-transfer reagents, as outlined in Figure 6. The

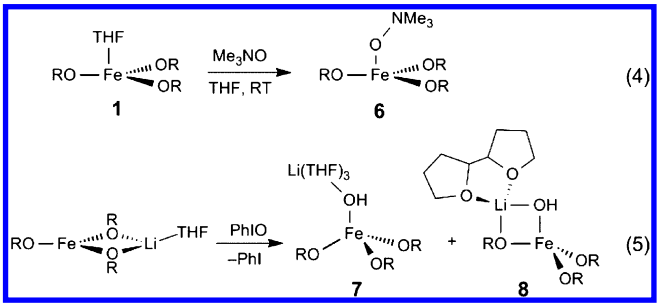


**Figure 6.** Reactivity of trigonal Fe(III) ditox compounds with oxo transfer reagents.

Fe(III) complex, **1**, did not exhibit any reactivity with iodosylbenzene (PhIO) over the course of a week at room temperature. In contrast, **1** reacted immediately with $Me_3NO$ but not in an oxidative transformation but rather to replace the apical THF to furnish **6**. The structure of **6** (Supporting Information, Figure S1) exhibits pseudo-tetrahedral geometry at the Fe(III) center, which is ligated by three ditox ligand and $ONMe_3$. The N−O bond distance in **6** is 1.397(2) Å, which falls within a usual range of values (1.38−1.40 Å) found for unactivated $ONMe_3$ (as provided by a CSD search that delivered 32 structures).[39−41]

Unlike **1**, compound **3** reacts with PhIO in THF at room temperature with facility. Dissolution of solid PhIO causes solutions of **3** to turn from pale green to pale yellow within about 30 s. In the absence of the Fe(II) complex, no dissolution of PhIO is observed within several hours. Fractional recrystallization of the oxidation products (from pentane and ether/THF phases) yielded two Fe(III)−hydroxide products in 25% and 23% yields, respectively: **7**, $[Fe(ditox)_3(OH)Li(THF)_3]$ with three THF molecules filling the coordination environment around the litium cation; and, **8**, $Fe(ditox)_3(\mu_2\text{-}OH)Li(C_8O_2H_{14})$ with a coupled THF chelate that coordinates to Li. Structures of the compounds **7** and **8**, shown in Figures 7 and 8, respectively, feature a distorted tetrahedral geometry at the metal centers. Both compounds display the expected OH stretch in the IR spectra (3700 $cm^{-1}$ and 3630 $cm^{-1}$, Supporting Information, Figures 12 and 14, respectively). Compound **8** is especially noteworthy, as it contains the 2,2′-bitetrahydrofuran ligand, which is also evident in ESI-MS. 2,2′-bi-THF has been previously prepared from THF via H-abstraction using radical reagents.[42,43]

Chemical analysis of **7** is complicated by the variability of the coordination environment imposed by Li, as shown in Figure 9. Drying compound **7** under vacuum led to a partial loss of THF to yield a solid mixture of **7** and **7a**, $Fe(ditox)_3(\mu_2\text{-}OH)Li(THF)_2$. Although **7a** and **7** are not easily separated from each other, we were able to discern the identity of **7a** by the single crystal XRD (from the bulk sample of **7**). The crystal structure of **7a** is shown in the Supporting Information, Figure S2. Compound **7a** differs from compound **7** in that it only has two THF molecules coordinated to the lithium cation as well as one Fe-bound alkoxide in a manner analogous to the connectivity observed in **8**. Unlike **8**, Compound **7a** has two


dx.doi.org/10.1021/ic302634q | Inorg. Chem. XXXX, XXX, XXX−XXX

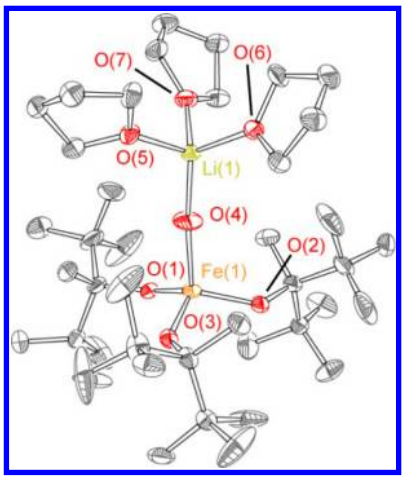


**Figure 7.** Structure of $Fe(ditox)_3(OH)Li(THF)_3$, (**7**), 30% probability ellipsoids. H atoms, co-crystallized solvent molecules, and alternative conformations of $^t$Bu groups are omitted for clarity. Selected bond distances: $d$(Fe1−O1) = 1.842(5) Å, $d$(Fe1−O2) = 1.860(4) Å, $d$(Fe1−O3) = 1.850(5) Å, $d$(Fe1−O4) = 1.945(5) Å, $d$(Li1−O4) = 1.794(11) Å. Selected bond angles: ∠(O1−Fe1−O2) =111.2(2)°, ∠(O1−Fe1−O3) = 111.4(2)°, ∠(O2−Fe1−O3) = 110.9(2)°, ∠(O1−Fe1−O4) = 107.4(3)°, ∠(O2−Fe1−O4) = 109.5(2)°, ∠(O3−Fe1−O4) = 106.3(3)°, ∠(Fe1−O4−Li1) 173.5(6)°.

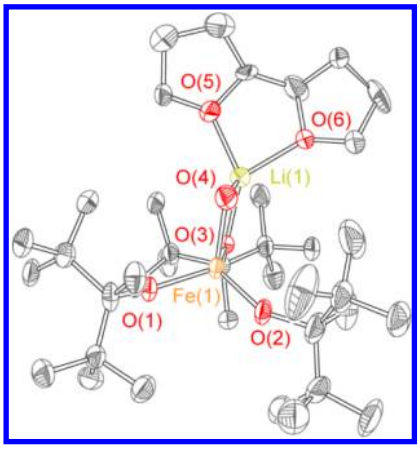


**Figure 8.** Structure of $Fe(ditox)_3(OH)Li(C_8O_2H_{14})$, (**8**), 50% probability. H atoms and alternative conformations of $^t$Bu groups are omitted for clarity. Selected bond distance: $d$(Fe1−O1) = 1.836(2) Å, $d$(Fe1−O2) = 1.823(2) Å, $d$(Fe1−O3) = 1.919(2) Å, $d$(Fe1−O4) = 1.920(2) Å, $d$(Li1−O3) = 1.949(5) Å, $d$(Li1−O4) = 1.885(7) Å, $d$(Li1−O5) = 1.995(5) Å, $d$(Li1−O6) = 2.014(5) Å. Selected bond angles: ∠(O1−Fe−O2) = 111.4(1)°, ∠(O1−Fe1−O3) = 111.5(1)°, ∠(O2−Fe1−O3) = 121.8(1)°, ∠(O1−Fe1−O4) = 111.4(1)°, ∠(O2−Fe1−O4) = 110.6(1)°, ∠(O3−Fe1−O4) = 87.9(1)°, ∠(O3−Li1−O4) = 88.0(2)°. The analogous structure with uncoupled THF molecules, **7a**, is shown in the Supporting Information, Figure S2.

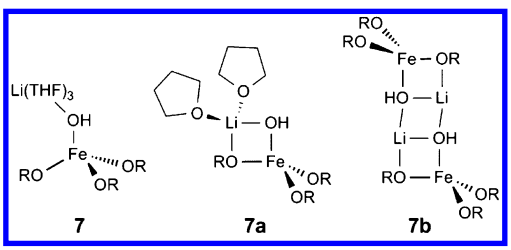


**Figure 9.** Solvation state differences for $Fe(ditox)_3(OH)Li$.

THF molecules which are uncoupled ligated to the lithium cation. The structural concordance of **7a** and **8** may explain the similarity in the OH stretching frequency of **7a** (Supporting Information, Figure S13) and **8**, about 3630 $cm^{-1}$, as opposed to that of **7**, which has an OH stretching frequency at 3700 $cm^{-1}$. ESI-MS of both **7a** and **8** show peaks consistent with the $[Fe(ditox)_3(OH)]^-$ ($m/z$ = 544.4) and $[Fe(ditox)_3(OH)(OH_2)]^-$ ($m/z$ = 562.4) ions. Exposure of the bright yellow transparent crystals of **7** to vacuum leads to an immediate loss of crystallinity.

Recrystallization of **7** in the absence of THF affords crystals of $[Fe(ditox)_3(OH)Li]_2$ (**7b**) (Supporting Information, Figure S3) in low yield. Compound **7b** differs from **7** and **7a** in that no solvent molecules are bound to the lithium cation. To complete the coordination environment around the lithium cation, **7b** effectively dimerizes to give "$Fe(ditox)_3(OH)Li$" units. Each Li atom has a coordination number of three that is achieved by its coordination to two hydroxide ligands and one Fe-bound alkoxide.

Eventual formation of an Fe(III)-OH complex via an oxygen atom transfer (OAT), and possible formation of an oxidized intermediate, is accompanied by formal hydrogen atom abstraction. Such reactivity is displayed by the oxidation of **5** to yield a terminal Fe(III)-OH moiety (**9**). The structure of **9** (Figure 10) is noteworthy, as the terminal hydroxide is

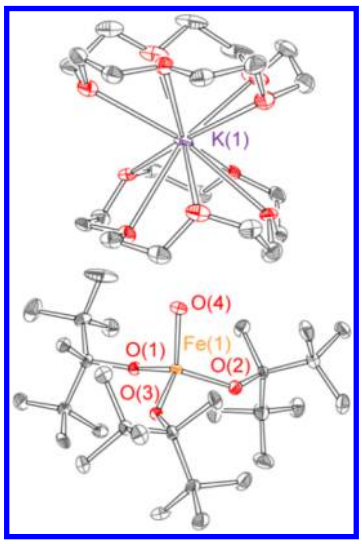


**Figure 10.** Structure $[Fe(ditox)_3(OH)][K(15C5)_2]$, (**9**), 50% probability ellipsoids. H atoms are omitted for clarity. Selected bond distances: $d$(Fe1−O1) = 1.868(2) Å, $d$(Fe1−O2) = 1.859(1) Å, $d$(Fe1−O3) = 1.859(1) Å, $d$(Fe1−O4) = 1.890(1) Å. Selected bond angles: ∠(O1−Fe1−O2) = 108.0(1)°, ∠(O1−Fe1−O3) = 111.1(1)°, ∠(O2−Fe1−O3) = 109.2(1)°, ∠(O1−Fe1−O4) = 110.0(0)°, ∠(O2−Fe1−O4) = 111.4(1)°, ∠(O3−Fe1−O4) = 107.2(2)°.

completely embedded inside the crown ether. The absence of an OH stretching frequency in the FTIR spectrum of **9** is likely due to strong hydrogen bonding to the 15-crown-5-ether. A distance of 3.20 Å between the oxygen of the metal bound hydroxide and an oxygen atom on the 15-crown-5-ether ring is consistent with a hydrogen bonding model.

To determine the source of the hydroxyl proton, the OAT reaction was performed in THF-$d_8$. Reaction in deutero-THF yielded both OH and OD, in about 50:50 ratio as determined by IR (Supporting Information, Figure S17). The deuteration of the hydroxide confirms that THF is a prominent source of


dx.doi.org/10.1021/ic302634q | Inorg. Chem. XXXX, XXX, XXX−XXX

the H atom. However, the presence of the protio form also suggests that the abstracted H atom can originate or be mediated by other sources of hydrogen atoms, such as advantageous water, glassware, or a $^{t}$Bu group of a ditox ligand located in a vicinity of the apical position. The ligand may possibly mediate H-atom transfer (oxidized intermediate abstracts H-atom from ligand generating a radical on the ligand that subsequently abstracts an H-atom from solvent). However, no $^{2}$H signal was observed in the $^{2}$H NMR spectrum of the hydrolyzed ligand after oxidations were performed. Alternatively, the ditox ligand could be an additional H-atom source and not a mediator, as it does not incorporate any deuterium. The reaction in silylated glassware does not change the ratio of the products, implying that the H atom does not originate from the glass. Exchange of the proton on the metal bound hydroxide with trace water cannot be ruled out as well. Despite this ambiguity, approximately 50% deuterium incorporation indicates that hydrogen atom abstraction from solvent is the primary pathway for reactivity upon oxygen atom transfer. Performing the OAT reaction in the presence of compounds possessing weak C−H bonds (e.g., 1,4−cyclohexadiene) yields **7** in isolated yields of about 90%.

Complete atom transfer to the Fe(II) center would produce a Fe(IV)-oxo intermediate, [Fe(IV)(ditox)$_3$(O)]$^-$. Accordingly, efforts were pursued to isolate or observe an Fe(IV)-oxo intermediate under a variety of reaction conditions. Temperatures were investigated as low as −78 °C. However, the formation of the Fe(III)-OH was instantaneous with mixing. The oxidative potency of the intermediate is further in evidence by its indiscriminate reaction with solvent. The formation of Fe(III)-OH complexes (both compounds **7** and **9**) is immediate even when solvents are used that possess thermodynamically strong C−H bonds (pentane, cyclohexane, and benzene). Whereas Fe(IV)-oxo intermediates are often able to be observed via in situ generation of the oxo in acetonitrile at cold temperatures,[7,8,18] in the case of **5**, the oxidative intermediate reacts with acetonitrile at −40 °C to furnish the C−H activation product, [Fe(ditox)$_3$(H$_2$CCN)]-[K(15C5)$_2$] (**10**), which was isolated and structurally characterized (Supporting Information, Figure S5). In addition to this C−H activated acetonitrile complex, FTIR of the reaction mixture shows the presence of Fe(III)-OH product **9**, indicating that C−H abstraction from CH$_3$CN by the oxidative intermediate is a likely reaction pathway. **9** does not react with CH$_3$CN, ruling out that **10** is produced from **9** and CH$_3$CN.

The oxidized intermediate can be intercepted with selected substrates. Oxidations of phosphines to phosphine oxides by amine-N-oxides have been shown to be prohibitively slow. For example, pyridine-N-oxide is unable to oxidize phosphines in the absence of a metal catalyst.[44] Fe(II)-ditox precursors treated with Me$_3$NO oxidize Ph$_3$P. Ph$_3$PO is immediately observed by $^{31}$P NMR in 80% yield (per mole of Me$_3$NO added) when **4** or **5** in 1,2-difluorobenzene is treated with Me$_3$NO in the presence of Ph$_3$P. This reaction is catalytic as treatment of 1 equiv of **4** with 10 equiv of NMe$_3$O and 10 equiv of PPh$_3$ shows formation of 7.5 equiv of PPh$_3$O. When THF is used as a solvent under similar conditions, the yield of the PPh$_3$O diminishes to about 20%. We attribute this decrease in phosphine oxidation to competitive hydrogen atom abstraction with the C−H bond of THF. This contention is supported by the observation of Fe(III)-OH stretching vibrations in the FTIR of the reaction mixture. These results together suggest a common intermediate for phosphine oxidation and hydrogen atom abstraction.

**Computational Chemistry.** DFT calculations at the B3LYP level using the Gaussian 03 suite were performed to assess the viability of a Fe(IV)-oxo intermediate. We utilized models of the putative Fe(IV)-oxo, **7** and **8**, where the ditox ligands are replaced by $^{t}$BuO$^-$ groups to simplify the computation. This simplification has been found to provide accurate and reliable results with similar types of compounds[29]

Our initial computational efforts focused on the electronic structure of a tris(alkoxide) Fe(IV)-oxo complex. We calculated two models: one as the free Fe(IV)-oxo anion, [Fe(O$^{t}$Bu)$_3$(O)]$^-$ (**A**), and the other as the neutral complex with an associated lithium cation, Li[Fe(O$^{t}$Bu)$_3$(O)] (**B**). The electronic structure of each of these models was probed for its appropriate ground state multiplicity. The energies of the singlet, triplet, and quintet states were computed while relaxing the geometry to their basal state. We found that the quintet state was the most stable for both the **A** and **B** as compared to the singlet and triplet states (Table 1). This result is in agreement with the prediction that a weak equatorial ligand field should favor high spin states and poor ancillary donor ligands should destabilize the high valent oxo state.[45]

**Table 1. Calculated Multiplicities, Selected Parameters, and Relative Energies Referenced to the Quintet State Respectively for [Fe(O$^{t}$Bu)$_3$(O)]$^-$ (A) and [Fe(OtBu)$_3$(O)Li] (B)**

| | | $d$(Fe−O$_{oxo}$)$_{avg}$ | $d$(Fe−O$_{alk}$)$_{avg}$ | rel. energy (kcal/mol) |
|---|---|---|---|---|
| **A** | quintet | 1.63 Å | 1.86 Å | 0 |
| | triplet | 1.61 Å | 1.87 Å | +13 |
| | singlet | 1.58 Å | 1.81 Å | +12 |
| **B** | quintet | 1.68 Å | 1.80 Å | 0 |
| | triplet | 1.70 Å | 1.78 Å | +21 |
| | singlet | 1.65 Å | 1.74 Å | +19 |

The optimized geometry of the anionic quintet state predicts a $d$(Fe-oxo) distance of 1.63 Å, which is in good agreement with experimentally found Fe(IV)-oxo bond distances. Analysis of the ancillary ligand environment of the quintet, triplet, and singlet spin states indicates that to stabilize lower spin states, $d$(Fe−O$_{alk}$) bond distances must shorten and ∠O$_{alk}$−Fe−O$_{alk}$ must be constricted relative to tetrahedral bond angles. These geometrical distortions are exacerbated by the increased steric bulk afforded by ditox relative to $^{t}$BuO$^-$. Therefore, it is likely that the quintet state of [Fe(ditox)$_3$(O)]$^-$ is even more stabilized relative to the computed model **A**.

The electronic structure of the **A** follows from an orbital parentage that is similar to the previously reported Cr(ditox)$_3$(O) analogue.[29] The frontier orbitals of the quintet state models have significant d-orbital character. The four singly occupied molecular orbitals (SOMOs) correspond to the doubly degenerate sets of $d_{xz}$ and $d_{yz}$, and $d_{xy}$ and $d_{x^2-y^2}$ (Figure 11). A significant amount of spin density (14%) is found to reside on the oxygen atom, due to the substantial oxo orbital character in the SOMOs.

The neutral model **B** shows that the quintet state model is further stabilized compared to the singlet and triplet states by 19 and 21 kcal/mol, respectively. The lithium cation is found between the oxygen atom from the oxo functional group and an oxygen atom from the alkoxide. The calculated $d$(Fe-oxo) bond distance of the neutral quintet state is predicted to be 1.68 Å.


dx.doi.org/10.1021/ic302634q | Inorg. Chem. XXXX, XXX, XXX−XXX

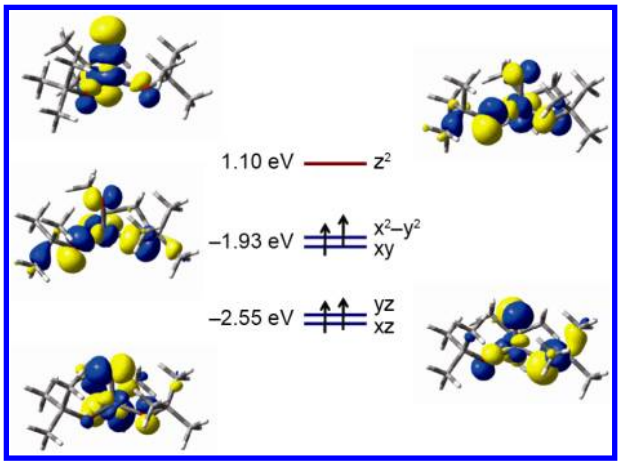


**Figure 11.** Molecular orbital diagram of the quintet ground state of $[Fe(O^tBu)_3(O)]^-$ for the $\alpha$ orbitals shown with an isovalue of 0.4.

The electronic structure of neutral **B** quintet state model is similar to that of the free anionic model where the SOMOs correspond to the doubly degenerate sets of ($d_{xz}$, $d_{yz}$) and ($d_{xy}$, $d_{x^2-y^2}$). The quintet model of **B** shows that significant radical O character from the oxo group is also observed in the SOMOs (Supporting Information, Figure S29) although the radical character in the $d_{xy}$ and $d_{x^2-y^2}$ orbitals is slightly attenuated compared to the Li-free anionic model (Supporting Information, Tables S2 and S3).

We also wished to estimate a possible mechanistic pathway for the activation of THF as observed experimentally (vide supra). A simple solvation model with one THF molecule was targeted for its relative ease of computation. Similar to the unsolvated Li[Fe(IV)-oxo] model **B**, the structure with one THF coordinated to the lithium cation, Li[Fe(IV)-oxo]THF, has a ground state optimized geometry with the lithium cation situated between the oxygen atom from the oxo group and an oxygen atom from an alkoxide. However, single crystal XRD data of $Fe(ditox)_3(OH)Li(THF)_3$ shows a different structural conformation with the lithium cation coordinated to the terminal hydroxide and solvent molecules, not the alkoxides. Additionally, structural data of $Cr(ditox)_3(O)K(Et_2O)_3$ does not show the alkali cation coordinated to an alkoxide ligand as the potassium coordinates to the terminal oxo and three solvent molecules exclusively. The similarity of these experimentally characterized analogous compounds supports the belief that in practical solvent environments a conformation in which the lithium cation is not interacting with the alkoxides is the ground state (Figure 12, Left). As such, the ground state structure of $Fe(O^tBu)_3(O)Li(THF)$ will be taken to be without the lithium cation coordinated to the alkoxide ligand.

With knowledge of the nature of the initial ground state, a reaction coordinate for C−H bond activation of THF via a high valent $Fe(O^tBu)_3(O)Li$ complex was calculated and is fully presented in Supporting Information, Figure S31. A transition state structure for C−H bond activation was determined (Figure 12, right), and the calculated transition state is found to include an $\alpha$-H from the solvated THF activated to produce a loosely associated Fe−OH moiety. This transition state structure is the lowest energy barrier toward C−H bond activation and lies at an accessible 7.6 kcal/mol higher than ground state. A radical intermediate structure is calculated along the reaction coordinate with a fully formed Fe(III)-OH functionality along with a radical localized on the THF

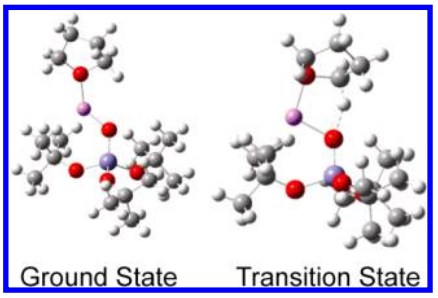


**Figure 12.** Optimized structures for the ground state geometry of $Fe(O^tBu)_3(O)Li(THF)$ and the corresponding transition state for hydrogen atom abstraction from $\alpha$ carbon of the coordinated THF.

associated to the lithium cation. The organic THF radical intermediate can be easily envisioned to react with a second THF radical to produce the bis-THF adduct **8**. This calculated mechanism provides an accessible pathway for the observed THF activation.

## DISCUSSION

The reported metathetical preparation and characterization of **1**−**5** represent a successful return to the original synthetic strategy employed by Thiessen and Koerner, who first isolated a homoleptic Fe(III)-alkoxide by the treatment of ferric chloride with sodium ethoxide.[46] Iron-alkoxide complexes have historically been difficult to isolate in a monometallic form because the alkoxide tends to engender multimetallic species by assuming a bridging coordination between metals.[47] The facile isolation of rare monomeric iron-tris(alkoxide) complexes reported here shows that proper tuning of the steric bulk of the alkoxide ligand is an effective strategy for discouraging the formation of multimetallic complexes, a feature that has plagued the alkoxide coordination chemistry.

Owing to the dearth of structurally characterized homoleptic iron-tris(alkoxide) complexes, it is difficult to thoroughly compare the observed metric parameters of **1**−**5** to other compounds. Two examplars of Fe(II) or Fe(III) tris(alkoxide) complexes have been structurally characterized. Cantalupo and co-workers have shown that the Fe(II) center of $Fe(OC_4F_9)_3K$-$(18\text{-crown-}6)_2$[48] is three coordinate with the $K^+$ cation coordinating to two of the fluorinated alkoxide ligands. An $Fe(OAr)_3$ aryloxide complex (Ar = 2,6, diphenylbenzene) has been structurally characterized as well.[49] The $d(Fe-O_{alk})$ bond distances of **3** and **4** are uniformly shorter than those of $Fe(OC_4F_9)_3K(18\text{-crown-}6)_2$ by approximately 0.05 Å. This indicates stronger bonding interactions between the iron and the alkoxides in **3** and **4**, which is likely important in stabilizing compounds **1**−**5** by discouraging ligand disproportionation and formation of tetrakis(alkoxide) complexes.

Iron(II) ditox complexes in the presence of OAT reagents exhibit unparalleled activity. All observed products including the formation of the Fe(III)-OH and the 2,2′-bi-tetrahydrofuran ligand products is consistent with H-atom abstraction by a Fe(IV)-oxo intermediate. However, we cannot rule out an alternative mechanism similar to the one proposed for Mn-corroles,[50] in which the oxidant species is actually the PhIO adduct of Fe(II). Regardless of the precise nature of the intermediate, the observed oxidation chemistry of **2**−**5** in the presence of OAT reagents is distinguished by exceptionally fast rates of reaction and by the indiscriminate nature in which hydrogen atom transfer occurs. One challenge with identifying the oxidative intermediate is its exceptional reactivity.


dx.doi.org/10.1021/ic302634q | Inorg. Chem. XXXX, XXX, XXX−XXX

Established procedures for observing Fe(IV)-oxo complexes typically involves the utilization of acetonitrile as a solvent at low temperatures. However, compounds **2**−**5** all furnish Fe(III)-OH as well as C−H activated products such as **10**, $[Fe(ditox)_3(CH_2CN)][K(15C5)_2]$ in acetonitrile at temperatures as low as −40 °C. This reactivity contrasts the chemistry of typical Fe-oxo complexes that are capable of activating substrates possessing BDEs as high as 110 kcal/mol but fail to do so for kinetic reasons.[51−53] For example, based on the empirical Evans−Polanyi relationship, though $[(N4Py)Fe^{IV}(O)]^{2+}$ should react with a C−H bonds possessing BDE of 95 kcal/mol at a rate of $\sim 10^{-4}$ $M^{-1}$ $s^{-1}$, the complex does not react with acetonitrile.[9,10,54,55] Similarly, the Evans−Polanyi relationship predicts that $[(bpy)_2(py)Ru(O)]^{2+}$ should react with C−H bonds of a BDE of 95 kcal/mol at a rate of $10^{-5}$ $M^{-1}$ $s^{-1}$. But no reaction with acetonitrile is observed despite the much greater concentration of neat acetonitrile as compared to substrate.[56,57] On this basis, the reaction rates of typical Fe-oxo compounds can conservatively be estimated to react with acetonitrile at rates that are least 2 orders of magnitude slower than what is expected based on the BDE of acetonitrile. Conversely, UV−vis spectra of reaction mixtures of Fe(II)-ditox complexes in the presence of OAT reagents show complete conversion to product in approximately a second. If one assumes reaction by pseudo first order kinetics, the reaction rates for the oxidative intermediate can be estimated utilizing the Eyring equation and the relationship $k = \ln(2)/t_{1/2}$. If a complete reaction is taken to represent seven half-lives (99.2% complete), a pseudo first order rate constant of approximately 10 $s^{-1}$ is obtained. Admittedly, this is a crude estimate of the rate constant for reaction, but it is in accordance with the instantaneous reactions observed at low temperatures as well as the low activation barrier calculated found from transition state DFT calculations (~8 kcal/mol).

The exceptional reactivity of Fe-ditox compounds with acetonitrile under oxidizing conditions is ascribed to steric and electronic factors. A clear rate dependence on steric crowding about Fe enforced by the ancillary ligand has been observed by Que and co-workers.[25] Using the structure of **9** as a guidepost, a space filling model can be generated that shows a potentially accessible axial coordination site in which the Fe-oxo or Fe-OAT adduct could reside within the ditox platform (Figure 13).

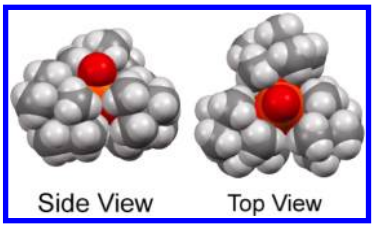


**Figure 13.** Space filling models of **9** depicting the accessibility of an apical oxygen atom (red) in a pseudo-tetrahedral geometry.

Whereas the exact Fe−O bond distance shown in the space filling model is too long for an Fe-oxo by 0.3 Å, the pseudo-tetrahedral geometry is similar to that of the structurally characterized early metal-oxo complexes in tris(ditox) ligand environments.[29] The model shows that the steric bulk of the ditox ligands is directed away from the axial coodination environment, thus providing insight as to the exceptional reactivity of the putative pseudo-tetrahedral Fe-tris(ditox) intermediate. Thus, the manner in which the steric bulk of the ligands is seen to not be directed toward the terminal oxygen atom does accurately model an accessible axial position toward substrates for a pseudo-tetrahedral Fe−tris(ditox) system.

Electronic structure calculations support enhanced reaction rates, particularly for an oxidizing intermediate in which OAT is complete. The weak ligand field of ditox together with a pseudo-tetrahedral environment engenders a high spin quintet state for a Fe(IV)-oxo intermediate. In addition, the ligand field orthogonal to the Fe-oxo bond ($d_{xy}$, $d_{x^2-y^2}$) is thought to promote high spin behavior.[45] Accessibility of such a high spin state has been shown to increase reaction rates.[22] Theoretical predictions by Neese directly correlate the accessibility of high spin states in Fe(IV)-oxo complexes to the ligand field strength orthogonal to the metal-oxo bond axis.

Calculations of early metal-oxo complexes supported by a tris(ditox) ancillary ligand field show that the primary interaction between the metal and the alkoxide is a $\sigma$ $p(O_{alk})-d_{xy}$, $d_{x^2-y^2}(M)$ bond; essentially identical to the primary bonding motifs in a trigonal bipyramidal geometry. Thus, by lowering the ancillary ligands below the $x/y$ plane, the pseudo-tetrahedral geometry creates poor orbital overlap with the $d_{xy}$, $d_{x^2-y^2}$ causing these orbitals to be lower in energy relative to pseudo-octahedral and pseudo-trigonal bipyramidal geometries. This in turn favors electronic population of $d_{xy}$, and $d_{x^2-y^2}$ over pairing electrons in $d_{xz}$ and $d_{yz}$ resulting in stabilization of a high spin state.

A weak ligand field orthogonal to the Fe-oxo bond axis could be essential to the high reactivity observed in the oxidized Fe-ditox system as well as explain the highly reactive nature of an Fe(III)-oxo recently reported by Smith and co-workers.[58] Smith's transient pseudo-tetrahedral Fe(III)-oxo is reported to be more difficult to isolate than many Fe(V)-oxo complexes and Fe(IV)-oxo complexes while performing similar C−H bond activation and OAT chemistries.[59] Our report of iron in a tris(ditox) ligand platform supports the emerging trend of the importance of high spin states induced by ancillary ligand fields in Fe-oxo complexes, possible over high oxidation states, as the contributing factor to highly reactive and difficult to isolate metal-oxo complexes.[16−18,24−26,56,57]

## CONCLUSIONS

An oxygen-rich pseudo-tetrahedral coordination sphere with strong $\pi$-donation is appealing as it engenders an extremely weak ligand field as compared to tetragonal nitrogen-donor coordination environments. Toward this end, we have prepared divalent and trivalent iron supported within the trigonal tris(alkoxide) platform. Alkoxide ligands typically have been ineffective at stabilizing three coordinate ancillary ligand fields because they are prone to bridging metals centers to result in multinuclear complexes.[60] While the use of the sterically crowded alkoxides has been shown to discourage the formation of bridging multinuclear species, they are typically too bulky to afford tris-alkoxide ancillary ligand spheres.[61] The ditox environment circumvents these issues to afford a trigonal, mononuclear Fe center predisposed to high spin states. Consistent with this contention, OAT to the Fe(II) ditox platform results in a oxidative intermediate that readily activates C−H bonds including those of solvents generally unreactive to high valent Fe-oxo compounds, especially those coordinated by nitrogen donor ligands in a tetragonal field. In summary, the steric and electronic factors of a tris(ditox) ligand field about


dx.doi.org/10.1021/ic302634q | Inorg. Chem. XXXX, XXX, XXX−XXX

iron together support exceptional oxidative reactivity. The limits of this reactivity will be explored in future studies.

## ■ ASSOCIATED CONTENT

### Supporting Information

IR spectra for complexes **1**−**10**, UV vis spectra for compounds **1**, **2**, **5**, and **9**, crystallographic details for complexes **1**−**10** and structures of **6**, **7a**, **7b**, **9**, and **10**. $^{31}$P NMR spectra for phosphine oxidation reactions. Computational details for $[Fe(O^tBu)_3(O)]^-$ and $LiFe(O^tBu)_3(O)$, calculated frontier orbital splitting diagrams, calculated spin density plots, and calculated transition state for H-atom abstraction. This material is available free of charge via the Internet at http://pubs.acs.org.

## ■ AUTHOR INFORMATION


### Corresponding Author

*E-mail: dnocera@fas.harvard.edu.

### Present Addresses

[§]Department of Chemistry, Wayne State University, Detroit Michigan 48202, United States.

[∥]Department of Chemistry, University of Texas at El Paso, El Paso, Texas 79968.


### Notes

The authors declare no competing financial interest.

## ■ ACKNOWLEDGMENTS

This research was supported by the NSF (Grant CHE-1112154). Grants from the NSF also provided instrument support to the DCIF at MIT (CHE−9808061, DBI−9729592. S.G. and D.V. acknowledge the support of the Dreyfus Foundation for Dreyfus Postdoctoral Fellowships in Environmental Chemistry. We thank Profs. C. C. Cummins and T. A. Betley for helpful discussions, and Dr. Wayne Lo for assistance with MS data.

## ■ REFERENCES


(1) Sono, M.; Roach, M. P.; Coulter, E. D.; Dawson, J. H. *Chem. Rev.* **1996**, *96*, 2841−2887.

(2) Meunier, B.; de Visser, S. P.; Shaik, S. *Chem. Rev.* **2004**, *104*, 3947−3980.

(3) Peloquin, J. M.; Campbell, K. A.; Randall, D. W.; Evanchik, M. A.; Pecoraro, V. L.; Armstrong, W. H.; Britt, R. D. *J. Am. Chem. Soc.* **2000**, *122*, 10926−10942.

(4) McEvoy, J. P.; Brudvig, G. W. *Chem. Rev.* **2006**, *106*, 4455−4483.

(5) Sun, C.-L.; Li, B.-J.; Shi, Z.-J. *Chem. Rev.* **2011**, *111*, 1293−1314.

(6) Holm, R. H. *Chem. Rev.* **1987**, *87*, 1401−1449.

(7) Nam, W. *Acc. Chem. Res.* **2007**, *40*, 522−531.

(8) Que, L., Jr. *Acc. Chem. Res.* **2007**, *40*, 493−500.

(9) Rohde, J.-U.; In, J.-H.; Lim, M. H.; Brennessel, W. W.; Bukowski, M. R.; Stubna, A.; Münck, E.; Nam, W.; Que, L., Jr. *Science* **2003**, *299*, 1037−1039.

(10) Lim, M. H.; Rohde, J.-U.; Stubna, A.; Bukowski, M. R.; Costas, M.; Ho, R. Y. N.; Münck, E.; Nam, W.; Que, L., Jr. *Proc. Natl. Acad. Sci. U.S.A.* **2003**, *100*, 3665−3670.

(11) Grapperhaus, C. A.; Mienert, B.; Bill, E.; Weyhermüller, T.; Wieghardt, K. *Inorg. Chem.* **2000**, *39*, 5306−5317.

(12) Klinker, E. J.; Kaizer, J.; Brennessel, W. W.; Woodrum, N. L.; Cramer, C. J.; Que, L., Jr. *Angew. Chem., Int. Ed.* **2005**, *44*, 3690−3694.

(13) de Visser, S. P.; Oh, K.; Han, A.-R.; Nam, W. *Inorg. Chem.* **2007**, *46*, 4632−4641.

(14) Hong, S.; Lee, Y.-M.; Cho, K.-B.; Sundaravel, K.; Cho, J.; Kim, M. J.; Shin, W.; Nam, W. *J. Am. Chem. Soc.* **2011**, *133*, 11876−11879.

(15) Harman, W. H.; Chang, C. J. *J. Am. Chem. Soc.* **2007**, *129*, 15128−15129.

(16) Lacy, D. C.; Gupta, R.; Stone, K. L.; Greaves, J.; Ziller, J. W.; Hendrich, M. P.; Borovik, A. S. *J. Am. Chem. Soc.* **2010**, *132*, 12188−12129.

(17) England, J.; Martinho, M.; Farquhar, E. R.; Frisch, J. R.; Bominaar, E. L.; Münck, E.; Que, L., Jr. *Angew. Chem., Int. Ed.* **2009**, *48*, 3622−3626.

(18) Bigi, J. P.; Harman, W. H.; Lassalle-Kaiser, B.; Robles, D. M.; Stich, T. A.; Yano, J.; Britt, R. D.; Chang, C. J. *J. Am. Chem. Soc.* **2012**, *134*, 1536−1542.

(19) Rohde, J.-U.; Stubna, A.; Bominaar, E. L.; Münck, E.; Nam, W.; Que, L., Jr. *Inorg. Chem.* **2006**, *45*, 6435−6445.

(20) Seo, M. S.; Kim, N. H.; Cho, K. B.; So, J. E.; Park, S. K.; Clémancey, M.; Garcia-Serres, R.; Latour, J.-M.; Shaik, S.; Nam, W. *Chem. Sci.* **2011**, *2*, 1039−1045.

(21) Ye, W.; Ho, D. M.; Friedle, S.; Palluccio, T. D.; Rybak-Akimova, E. V. *Inorg. Chem.* **2012**, *51*, 5006−5021.

(22) Hirao, H.; Kumar, D.; Que, L., Jr.; Shaik, S. *J. Am. Chem. Soc.* **2006**, *128*, 8590−8606.

(23) Janardanan, D.; Wang, Y.; Schyman, P.; Que, L., Jr.; Shaik, S. *Angew. Chem., Int. Ed.* **2010**, *49*, 3342−3345.

(24) England, J.; Guo, Y.; Farquhar, E. R.; Young, V. G.; Münck, E.; Que, L., Jr. *J. Am. Chem. Soc.* **2010**, *132*, 8635−8644.

(25) England, J.; Guo, Y.; Van Heuvelen, K. M.; Cranswick, M. A.; Rohde, G. T.; Bominaar, E. L.; Münck, E.; Que, L., Jr. *J. Am. Chem. Soc.* **2011**, *133*, 11880−11883.

(26) Gupta, R.; Lacy, D. C.; Bominaar, E. L.; Borovik, A. S.; Hendrich, M. P. *J. Am. Chem. Soc.* **2012**, *134*, 9775−9784.

(27) Betley, T. A.; Wu, Q.; Van Voorhis, T.; Nocera, D. G. *Inorg. Chem.* **2008**, *47*, 1849−1861.

(28) Nocera, D. G. *Inorg. Chem.* **2009**, *48*, 10001−10007.

(29) Groysman, S.; Villagrán, D.; Nocera, D. G. *Inorg. Chem.* **2010**, *49*, 10759−10761.

(30) Wolczanski, P. T. *Polyhedron* **1995**, *14*, 3335−3362.

(31) Murray, B. D.; Power, P. P. *J. Am. Chem. Soc.* **1984**, *106*, 7011−7015.

(32) Evans, D. F. *J. Chem. Soc.* **1959**, 2003−2005.

(33) Napolitano, E.; Giovani, E.; Ceccarelli, N.; Pelosi, P. *J. Agric. Food Chem.* **1996**, *44*, 2806−2809.

(34) (a) Becke, A. D. *Phys. Rev. A* **1988**, *38*, 3098. (b) Becke, A. D. *J. Chem. Phys.* **1993**, *98*, 1372. (c) Becke, A. D. *J. Chem. Phys.* **1993**, *98*, 5648.

(35) Lee, C.; Yang, W.; Parr, R. G. *Phys Rev. B* **1988**, *37*, 785.

(36) Frisch, M. J.; Trucks, G. W.; Schlegel, H. B.; Scuseria, G. E.; Robb, M. A.; Cheeseman, J. R.; Montgomery, Jr., J. A.; Vreven, T.; Kudin, K. N.; Burant, J. C.; Millam, J. M.; Iyengar, S. S.; Tomasi, J.; Barone, V.; Mennucci, B.; Cossi, M.; Scalmani, G.; Rega, N.; Petersson, G. A.; Nakatsuji, H.; Hada, M.; Ehara, M.; Toyota, K.; Fukuda, R.; Hasegawa, J.; Ishida, M.; Nakajima, T.; Honda, Y.; Kitao, O.; Nakai, H.; Klene, M.; Li, X.; Knox, J. E.; Hratchian, H. P.; Cross, J. B.; Bakken, V.; Adamo, C.; Jaramillo, J.; Gomperts, R.; Stratmann, R. E.; Yazyev, O.; Austin, A. J.; Cammi, R.; Pomelli, C.; Ochterski, J. W.; Ayala, P. Y.; Morokuma, K.; Voth, G. A.; Salvador, P.; Dannenberg, J. J.; Zakrzewski, V. G.; Dapprich, S.; Daniels, A. D.; Strain, M. C.; Farkas, O.; Malick, D. K.; Rabuck, A. D.; Raghavachari, K.; Foresman, J. B.; Ortiz, J. V.; Cui, Q.; Baboul, A. G.; Clifford, S.; Cioslowski, J.; Stefanov, B. B.; Liu, G.; Liashenko, A.; Piskorz, P.; Komaromi, I.; Martin, R. L.; Fox, D. J.; Keith, T.; Al-Laham, M. A.; Peng, C. Y.; Nanayakkara, A.; Challacombe, M.; Gill, P. M. W.; Johnson, B.; Chen, W.; Wong, M. W.; Gonzalez, C.; and Pople, J. A. *Gaussian 03*, Revision C.02; Gaussian, Inc.: Wallingford, CT, 2004.

(37) (a) Wadt, W. R.; Hay, P. J. *J. Chem. Phys.* **1985**, *82*, 284. (b) Hay, P. J.; Wadt, W. R. *J. Chem. Phys.* **1985**, *82*, 299.

(38) (a) Dunning, T. H., Jr. *J. Chem. Phys.* **1989**, *90*, 1007. (b) Dunning, T. H.; Hay, P. J. In *Modern Theoretical Chemistry. 3. Methods of Electronic Structure Theory*; Schaefer, H. F., III, Ed.; Plenum Press: New York, 1977. (c) Woon, D. E.; Dunning, T. H. *J. Chem. Phys.* **1993**, *98*, 1358.

(39) Hong, S.; Gupta, A. K.; Tolman, W. B. *Inorg. Chem.* **2009**, *49*, 6323−6325.

(40) Caron, A.; Palenik, G. J.; Goldish, E.; Donohue, J. *Acta Crystallogr.* **1964**, *17*, 102−108.
(41) Jin, S.; Nieuwenhuyzen, M.; Robinson, W. T.; Wilkins, C. J. *Acta Crystallogr., Sect. C: Cryst. Struct. Commun.* **1992**, *48*, 274−279.
(42) Naarmann, H.; Beaujean, M.; Merényi, R.; Viehe, H. G. *Polym. Bull.* **1980**, *2*, 363−372.
(43) Brown, S. H.; Crabtree, R. H. *J. Am. Chem. Soc.* **1989**, *111*, 2935−2946.
(44) Cai, X.; Majumdar, S.; Fortman, G. C.; Frutos, L. M.; Temprado, M.; Clough, C. R.; Cummins, C. C.; Germain, M. E.; Palluccio, T.; Rybak-Akimova, E .V.; Captain, B.; Hoff, C. D. *Inorg. Chem.* **2011**, *50*, 9620−9630.
(45) Neese, F. *J. Inorg. Biochem.* **2006**, *100*, 716−726.
(46) Thiessen, P. A.; Koerner, O. *Z. Anorg. Chem.* **1929**, *180*, 65−74.
(47) Bradley, D. C.; Mehrotra, R. C.; Rothwell, I. P.; Singh, A. *Alkoxo and Aryloxo Derivatives of Metals*; Academic Press: London, U.K., 2001.
(48) Cantalupo, S. A.; Lum, J. S.; Buzzeo, M. C.; Moore, C.; DiPasquale, A. G.; Rheingold, A. L.; Doerrer, L. H. *Dalton Trans.* **2010**, *39*, 374−383.
(49) Boyle, T. J.; Ottley, L. A. M.; Apblett, C. A.; Stewart, C. A.; Hoppe, S. M.; Hawthorne, K. L.; Rodriguez, M. A. *Inorg. Chem.* **2011**, *50*, 6174−6182.
(50) Zdilla, M. J.; Abu-Omar, M. M. *Inorg. Chem.* **2008**, *47*, 10718−10722.
(51) Hodgkiss, J. M.; Rosenthal, J.; Nocera, D. G. The Relation between Hydrogen Atom Transfer and Proton-coupled Electron Transfer in Model Systems. In *Hydrogen-Transfer Reactions*; Hynes, J. T., Klinman, J. P., Limbach, H.-H., Schowen, R. L., Eds.; Wiley-VCH Verlag GmbH & Co. KGaA: Weinheim, Germany, 2007.
(52) Roelfes, G.; Lubben, M.; Hage, R.; Que, L., Jr.; Feringa, B. L. *Chem.—Eur. J.* **2000**, *6*, 2152−2159.
(53) Hirao, H.; Que, L., Jr.; Nam, W.; Shaik, S. *Chem.—Eur. J.* **2008**, *14*, 1740−1756.
(54) Decker, A.; Rhode, J. U.; Que, L., Jr.; Solomon, E. I. *J. Am. Chem. Soc.* **2004**, *126*, 5378−5379.
(55) Kaizer, J.; Klinker, E. J.; Oh, N. Y.; Rhode, J. U.; Songm, W. J.; Stubna, A.; Kim, J.; Munck, E.; Nam, W.; Que, L., Jr. *J. Am. Chem. Soc.* **2004**, *126*, 472−473.
(56) Bryant, J. R.; Mayer, J. M. *J. Am. Chem. Soc.* **2003**, *125*, 10351−10361.
(57) Bryant, J. R.; Matsuo, T.; Mayer, J. M. *Inorg. Chem.* **2004**, *43*, 1587−1592.
(58) Smith, J. M.; Mayberry, D. E.; Margarit, C. G.; Sutter, J.; Wang, H.; Meyer, K.; Bontchev, R. P. *J. Am. Chem. Soc.* **2012**, *134*, 6516−6519.
(59) McDonald, A. R.; Que Jr., L. *Coord. Chem. Rev.* **2013**, *257*, 414−428.
(60) Mehrotra, R. C. *Inorg. Chim. Acta, Rev.* **1967**, *1*, 99−112.
(61) Power, P. P. *J. Organomet. Chem.* **2004**, *689*, 3904−3919.